Spatial Ring Current Model of the [2.2]Paracyclophane Molecule

Stefano Pelloni,[†] Paolo Lazzeretti,*[,†] and Riccardo Zanasi[‡]

Dipartimento di Chimica dell'Università degli Studi di Modena e Reggio Emilia, Via Campi 183, 41100 Modena, Italy, and Dipartimento di Chimica dell'Università degli Studi di Salerno, via Ponte don Melillo, 84084 Fisciano (SA), Italy

Received: November 14, 2006

A representation of the current density induced in the [2.2]paracyclophane molecule by a homogeneous magnetic field parallel to the line joining the centers of the phenylene rings is given in compact form by a stagnation graph that conveys essential information. Analogous graphs were obtained for two perpendicular directions. Plots of streamlines are also reported to complete a ring current model that has been proved useful to understand the magnetropicity of the system. Stagnation graphs, maps of streamlines and moduli of the current density, and plots of Biot−Savart magnetic shielding density provide a basic tool kit for rationalizing magnetic response of complex systems.

1. Introduction

Cyclophanes contain two distorted phenylene moieties connected by short aliphatic bridges. These compounds are endowed with interesting chemical properties.[1−3] However, the aromatic character of cyclophanes is still a matter of discussion. Attempts have recently been made to assess the diatropicity of these species in terms of nucleus-independent chemical shift (NICS).[4−7] Caramori et al.[8] compared NICS calculated for [2.2]cyclophanes with those of benzene and xylene dimers. They found that superimposition of two aromatic rings causes NICS to decrease with respect to the free molecules along the inner portion of a line through their centers. Calculated values would imply that there is a concentration of electronic charge between the ring as a consequence of the bridging process.[8]

This conclusion was refuted by Poater et al.,[9] who claimed that the decrease of NICS should instead be imputed to a "magnetic coupling" between superimposed rings. These authors also warn about the use of NICS as an aromaticity indicator for compounds possessing closely packed phenylene groups.[9] In a related paper, investigating stacked polyfluorenes, Osuna et al.[10] still rely on the idea of magnetic coupling between stacked rings to account for changes of local aromaticity. However, the origin and the essential features of this coupling are not clear and, in our view, they should be explained in detail for an educated guess of magnetotropicity of the [2.2]paracyclophane molecule. This is the aim of the present paper.

Intuitively, one can say that juxtaposing two benzene rings at a sufficiently short distance from one another, in the presence of an external magnetic field, will induce significant deviations from the magnetic response of a single ring, owing to mutual influence. Nonetheless, to avoid nominalistic traps, appropriate quantum mechanical tools are to be employed for understanding the nature of the "coupling". The average NICS descriptor[4] is basically unsuitable to investigate the magnetic interaction between the two close phenylene rings of [2.2]paracyclophane, as demonstrated by actual calculations,[9] for the general reasons previously discussed in detail.[11,12] The "conceptual imperfections"[6,7] of the average NICS have been recognized. Other noticeable failures have been documented.[13−15] Neither can the out-of-plane component of the central magnetic shielding (usually indicated by $NICS_{zz}$), proposed for monocyclic molecules[12] and adopted later on,[5−7] be used with confidence for, e.g., a model system made up of two parallel benzene rings in the presence of a magnetic field **B** perpendicular to them.

Recent analyses clearly show that, in most cases, a local shielding value, i.e., a single number arrived at by the integral Biot−Savart law (BSL), is insufficient to decide whether a molecule is diatropic or not. Just the other way round, rigorous explanations of the effects of electron currents on nuclear magnetic shielding are obtained by plots of the shielding density function, that is, the integrand of the BSL.[16−20]

2. Three-Dimensional Ring Current Models via Stagnation Graphs

The phenomenology of a molecule in a magnetic field can, in principle, be fully understood if an accurate description of the subobservable[21] $\mathbf{J}^{\mathbf{B}}$, *i.e.*, the quantum current density vector, is available. Simple relationships of classical electrodynamics can then successfully be applied to interpret molecular magnetic properties in terms of $\mathbf{J}^{\mathbf{B}}$, say, the Ampere theorem for magnetizabilities and the BSL for nuclear magnetic shielding.[11,12,16,17,19,20] Therefore a *model of the induced current density vector field* is needed for a reliable assessment of the magnetotropicity of [2.2]cyclophanes. On the other hand, such a model, easy to obtain for planar conjugated systems,[13,22] is, according to our experience, more difficult to construct for stacked-ring species, e.g., [2.2]paracyclophane, which constitutes a stimulating challenge.

Recent studies report maps of the current density at points in the plane of a conjugated cyclic molecule, or in a plane parallel to it, in a region where the π-electron density is nearly maximum. This is usually enough to rationalize the magnetotropicity of most mono- and polycyclic systems in less difficult cases. However, plotting the current density only on a few reference planes is in general insufficient to show the spatial aspects of the electron flow all over the molecular domain,

* Corresponding author. E-mail: lazzeret@unimo.it.
[†] Dipartimento di Chimica dell'Universita degli Studi di Modena e Reggio Emilia.
[‡] Dipartimento di Chimica dell'Universita degli Studi di Salerno.

10.1021/jp067540o CCC: $37.00
Published on Web 03/29/2007

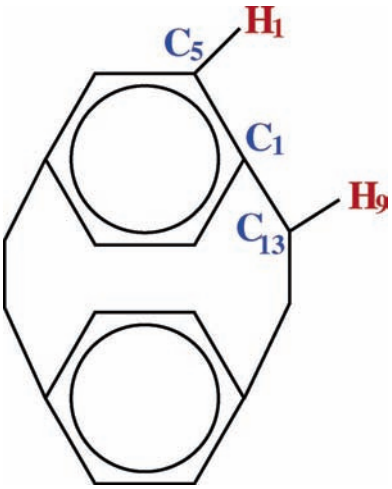

Figure 1. Numbering of symmetry-unique atoms in the [2.2]paracyclophane molecule.

which may cause incorrect interpretations. In other words, *the planar current models usually reported in the literature fail to account for the third dimension of the current density field*.

The magnetic shielding at a nucleus depends on the second inverse power of its distance from an element of current, therefore it is the flow nearby the probe that determines the bulk of the shielding. Thus statements currently made relying on planar models for the $\mathbf{J^B}$ field, e.g., that a probe nucleus over a diamagnetic π-ring current is shielded, although in principle correct, may be affected by systematic errors. Detailed information on what is going on in space is needed.

A description of the current density vector field induced in [2.2]paracyclophane by an external magnetic field parallel to the line connecting the centers of the phenylene rings, indispensable to interpret its magnetotropism, can in principle be obtained by plotting $\mathbf{J^B}$ on several planes perpendicular to **B**. However, the model so obtained would be impractical for at least two reasons: (i) important details may be overlooked, unless the series of planes is wide enough; (ii) it would carry too many pieces of information, difficult to assemble in a single mental picture.

As the most relevant features of $\mathbf{J^B}$ are observed in the proximity of its *singular point* at which the vector field vanishes (i.e., the electrons stop moving), portable and compact models of the current density field are available to interpret magnetic response via a *stagnation graph* (SG) showing the whole set of singular isolated points and lines.[23−25] Significant economy of thinking is achieved via ab initio SGs obtained for planar cyclic molecules, e.g., the aromatic C_nH_n rings,[11,26] and five-membered heterocycles.[27]

Mathematical aspects and technical details for plotting streamlines and modulus of current density, and SG, have been discussed at length elsewhere.[11,23−27] Phase portraits for singularities are shown in these papers; see, for instance, Figures 1 and 2 of ref 11. Vortices consist of closed loops that can be either diamagnetic or paramagnetic. Two close vortices may be separated by a saddle point. In its vicinity, the streamlines are approximately rectangular hyperbolae. Stagnation lines (SL) are continuous manifolds of stagnation points of the same type. They may be either vortical or saddle lines, connecting the singular points of a given type, i.e., vortices or saddles, observed in the streamline maps for planes at different heights along a vertical axis. Because SGs are complicated topological objects, a graphic software is available in the supporting material to observe their spatial features in three dimensions. The representations so obtained can be blown up and rotated for detailed inspection.[28] Use of this software, freely delivered by the authors, is recommended to understand the following discussion.

TABLE 1: Magnetic Properties of D_{2h} [2.2]Paracyclophane

method	*xx*	*yy*	*zz*	Av
	$\chi_{\alpha\beta}$ [ppm au]			
GIAO	−1060.3	−1047.0	−2769.4	−1625.6
CTOCD−PZ2	−1017.6	−998.0	−2708.6	−1574.7
	$\sigma^I_{\alpha\beta}$ [ppm]			
I				
C_1 (GIAO)	−61.0	5.5	172.6	39.0
C_5 (GIAO)	13.6	−44.4	173.1	47.4
C_{13} (GIAO)	171.0	139.6	161.8	157.4
H_1 (GIAO)	27.3	24.8	23.2	25.1
H_9 (GIAO)	29.8	29.2	27.9	29.0
C_1 (PZ2)	−61.8	5.0	169.9	37.7
C_5 (PZ2)	12.9	−44.8	171.7	46.6
C_{13} (PZ2)	168.1	137.5	159.3	155.0
H_1 (PZ2)	27.2	23.9	23.4	24.8
H_9 (PZ2)	29.3	29.0	27.7	28.7
	$\sigma_{\alpha\beta}$(**r**) [ppm] CTOCD−PZ2			
r(bohr)				
CM	−2.6	−5.5	50.2	14.0
x_2 (0.94)	−3.2	−3.5	49.7	14.3
x_3 (1.89)	−2.0	−2.5	41.9	12.5
x_4 (2.83)	3.6	−8.7	26.0	7.0
x_5 (3.78)	14.5	−7.3	19.8	9.0
x_6 (4.72)	36.5	28.8	33.2	32.8
x_7 (5.67)	41.0	34.5	39.5	38.0
x_8 (6.61)	21.3	−0.4	19.0	13.3
y_2 (0.94)	−2.4	−7.5	50.0	13.4
y_3 (1.89)	−1.8	−9.2	44.3	11.1
y_4 (2.83)	−0.9	−7.5	28.1	6.6
y_5 (3.78)	0.0	−4.0	10.8	2.3
z_2 (0.94)	−2.3	−9.2	44.3	10.9
z_3 (1.89)	−0.2	−4.0	10.8	2.2
z_4 (2.83)	−0.07	0.9	−2.5	−0.6
z_5 (3.78)	−0.5	1.8	−3.0	−0.6
z_6 (4.72)	−0.5	1.4	−2.1	−0.4

3. Details of Calculation

Molecular geometries for two model systems have been optimized at the B3LYP/6-31G** level of accuracy, using the GAUSSIAN98 code.[29] The first consists of two stacked benzene rings, the second corresponds to a D_{2h} structure of [2.2]-paracyclophane (Figure 1). As a matter of fact, a system with D_2 geometry is slightly more stable, the B3LYP/6-31G** energy for the D_{2h} (D_2) being −619.3237878 (−619.3426021) hartrees. On the other hand, calculated magnetic properties are virtually the same for the two geometries. A slightly idealized structure with higher symmetry guarantees more efficient use of the SYSMO code[30] and a graphic output much easier to read.

Magnetic properties have been calculated via a procedure using continuous transformation of the origin of the current density-paramagnetic zero (CTOCD-PZ2),[31] implemented in SYSMO, employing the (13s8p/8s) → [5s4p/4s] basis from van Duijneveldt[32] for C/H at the Hartree−Fock level. The s basis for C has been augmented by a diffuse function with exponent 0.0399. Two 3d functions, with exponents 2.1409 and 0.64240, and two 2p functions, with exponents 2.0731 and 0.49099, have been added on C and H, respectively, obtaining a [6s4p2d/4s2p] basis set. A London basis of gauge-including atomic orbitals (GIAO)[33] was constructed by adding gauge-phase factors to the gaugeless [6s4p2d/4s2p] basis set. The DALTON code[34] was employed to evaluate magnetic properties via the GIAO basis. The results obtained for magnetic susceptibility, magnetic

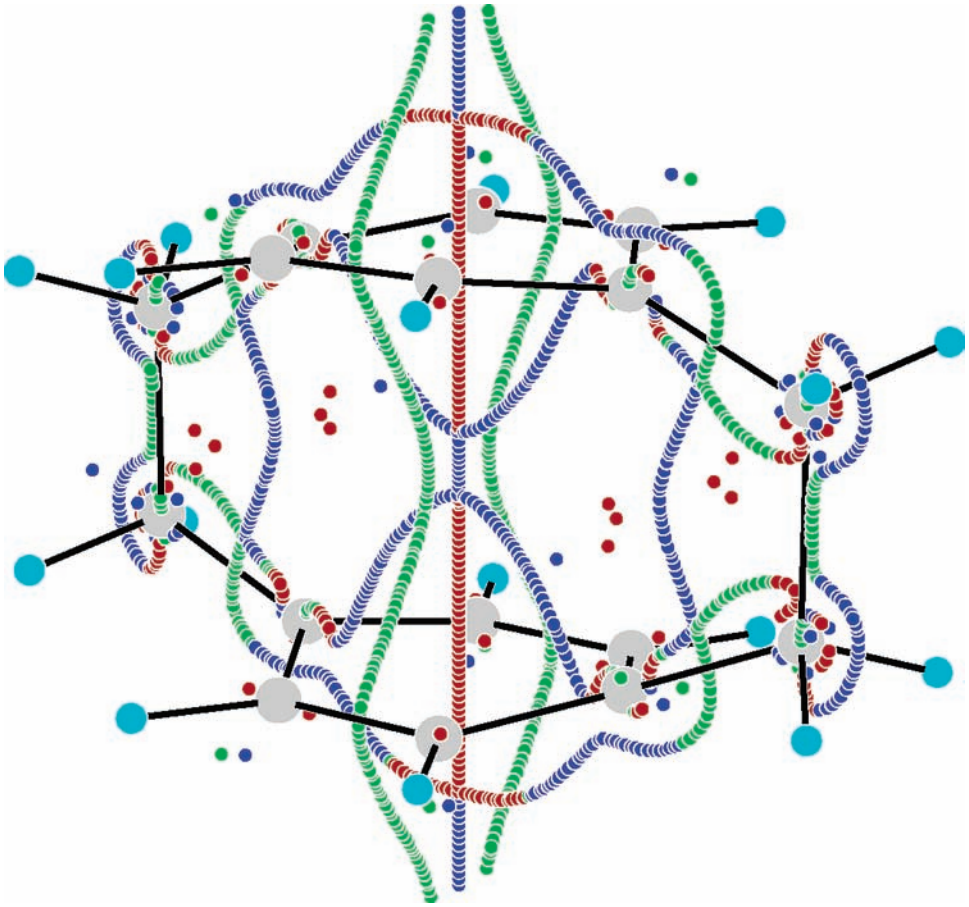

Figure 2. Perspective view of the stagnation graph of the current density vector field in [2.2]paracyclophane. The distance between the centers of the phenylene rings is ≈ 5.95 bohr. The uniform external magnetic field, $\mathbf{B} \equiv B\epsilon_3$, is parallel to the *z* axis through the centers of the phenylene rings. Green (red) lines denote diamagnetic (paramagnetic) vortices, saddle lines are blue.

shielding at C and H nuclei, and at few points along the *x*, *y*, and *z* directions, are reported in the Table 1. The good agreement between CTOCD-PZ2 and GIAO calculations guarantees the accuracy of the numerical estimates. The SG of [2.2]paracyclophane has been constructed within the CTOCD-DZ2 scheme[31] by a graphic software available in the SYSMO package[30] (i) for a magnetic field along the *z* axis, i.e., the direction through the centers of the phenylene rings, (i) for the *x* axis through the midpoints of the central C−C aliphatic bonds, and (iii) for the *y* axis, normal to the plane of the aliphatic bridges. The origin of the coordinate system lies at the CM.

4. Results and Discussion

4.1. Stagnation Graph for $\mathbf{B} \equiv B\epsilon_3$. To understand the essential aspects of the magnetic interaction between two stacked phenylene moieties, it is expedient to compare the SG of [2.2]-paracyclophane with that of a hypothetical molecule consisting of two superimposed benzene rings at a distance *d* sufficiently large that the magnetic interaction between the two stacked C_6H_6 molecules is small, assuming **B** normal to the ring planes. For $d \approx 6.62$ bohr, the SG of the latter looks like the superimposition of the SGs of two single rings,[16,26] see the Supporting Information. In comparison with that of [2.2]paracyclophane in Figure 2, it shows radical differences. In both cases, an SL, denoted as *primary*, connects the centers of the rings. This SL is *vortical* in the model for two stacked benzene rings. It is diamagnetic (green) along a segment through the center of mass CM and in the tail regions of the molecule, and it contains two paramagnetic (red) segments crossing each ring plane.

Quite remarkably, the central SL for [2.2]paracyclophane in Figure 2 is instead *saddle-like* in the outer regions of the molecular domain and along a short segment having the CM as midpoint. At the distance of $\approx \pm 0.4$ bohr from CM, the central SL splits into two saddle lines, lying on the *zx* plane, i.e., the plane of the C−C bridging bonds, and a central paramagnetic vortex line. Paramagnetic vortices flow through the phenylene groups as in the model system of two superimposed C_6H_6; compare with the SG in the Supporting Information. Therefore, the "paramagnetic core", typical of benzene rings,[11] is conserved on stacking them at short distances in [2.2]-paracyclophane. Further splitting of each paramagnetic vortex line into two paramagnetic vortical lines on the *zx* plane, and a saddle line extending beyond the phenylene rings, occurs at a couple of branching points, symmetrically placed above and below the benzene rings, at $\approx \pm 4.6$ bohr from the CM. A closed SL fully lying in the *zx* plane, and containing segments of different types, passes through these branching points. It surrounds the phenylene rings.

The splitting of the primary SL into other lines is regulated by topological rules.[23−25] Two diamagnetic vortices flow at the sides of the central SL. The corresponding green SLs, lying on the *yz* plane, pass through four C−C bonds of the phenylene rings. They extend to the tail regions of the molecule, approaching the central saddle SL. This set of SLs, a central saddle between two diamagnetic vortices, is quite typical. It occurs after the bifurcation of the primary diamagnetic vortical line in the far out part of the molecule at branching points $\pm Z$, not visible in Figure 2. In this region, i.e., for $|z| > Z$, the regime

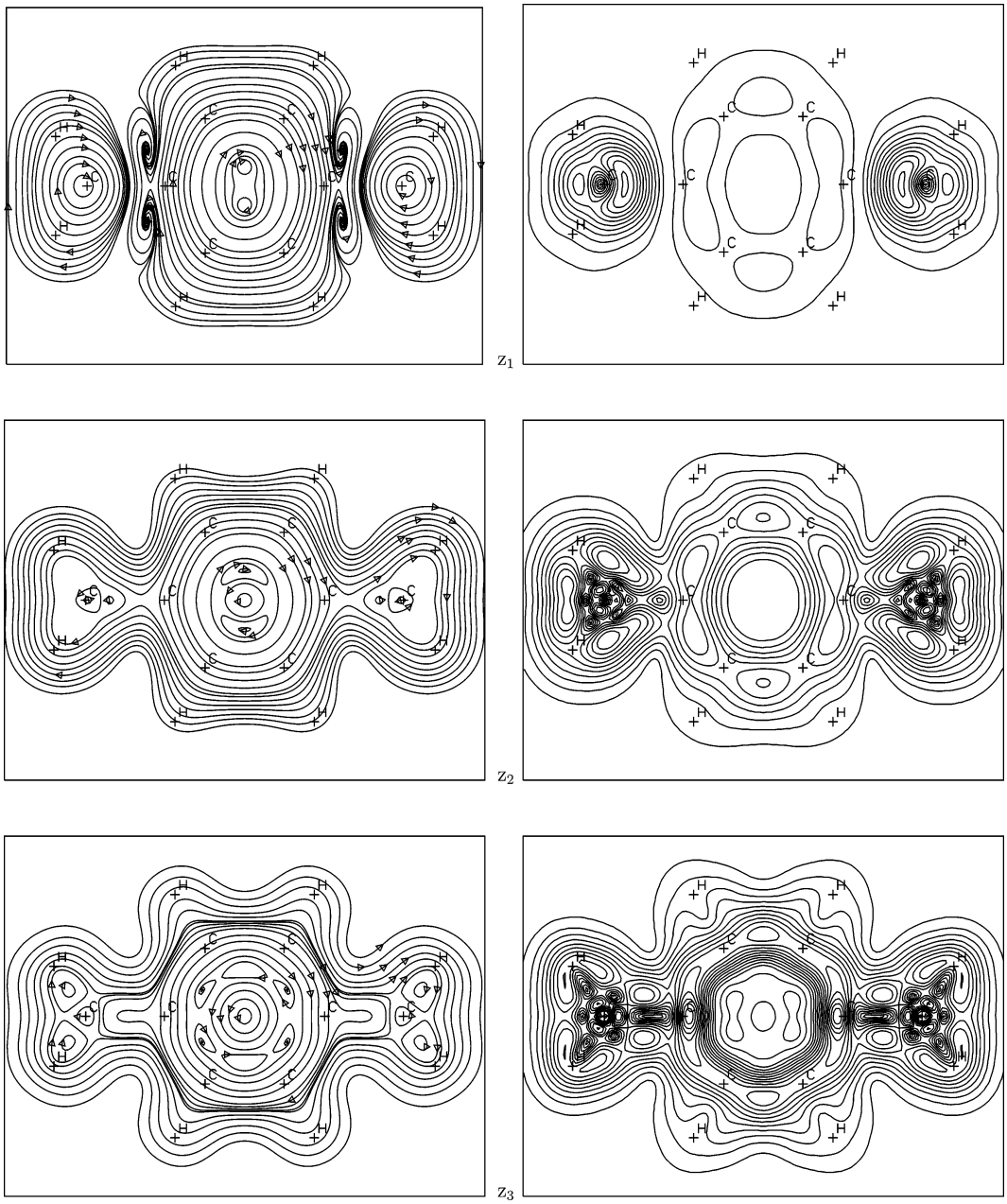

Figure 3. Streamlines (on the left) and contour levels for the modulus (on the right) of the current density $\mathbf{J^B}$ induced by a magnetic field $\mathbf{B} \equiv B\epsilon_3$ with intensity 1 au directed upward. On the *xy* plot planes, diamagnetic currents are clockwise. The distances z_i from the center of mass are specified in the Table. Atom positions are marked by crosses. The contours are associated with constant magnitude of $\mathbf{J^B}$, and are drawn from the initial value $|\mathbf{J^B}| = 0.0$ in steps of 4×10^{-3}, 4×10^{-3}, and 1×10^{-2} au to the maximum values 4.46×10^{-2}, 4.38×10^{-2}, and 1.48×10^{-1} au in the maps for z_1, z_2, and z_3, respectively.

is fully diamagnetic, resembling that of an atom. Symmetry is broken on approaching the molecular skeleton, and the external diamagnetic vortex splits up into two vortical lines at the sides and a central saddle line.

Such a pattern is very different from that observed in the model of superimposed C_6H_6 ring. Whereas six diamagnetic vortices flow across the C−C bonds in benzene (and in the hypothetical system of two packed noninteracting benzene rings, see the SG in the Supporting Information), only two diamagnetic vortices through four phenylene bonds survive in [2.2]paracyclophane. Therefore, one may conclude that close-packing via aliphatic bridges reduces the diatropicity of the system about the *z* axis.

The SG indicates where most significant planes can be searched to visualize an "economical" ring current model of [2.2]paracyclophane via a small set of $\mathbf{J^B}$ maps. The streamlines on *xy* planes perpendicular to the **B** field, at different distances from the CM, are shown in Figures 3 and 4. The results are fully consistent with the SG of Figure 2. The phase portrait of the central saddle is observed on the map at $z_1 = 0$ bohr of Figure 3 (the asymptotes through the saddle are not visible at the resolution adopted), in the proximity of the CM, coinciding with the midpoint of the segment that joins two small diamagnetic vortices. The two green vortical SLs at the sides of the central saddle SL in Figure 2 pass through their centers. This central pattern is contained within a wider region of diamagnetic vortical regime. Ring currents flow all around the projections of the C and H nuclei on the plot plane. Spiralling currents are observed on the sides of this central vortex. Two diamagnetic vortices flow nearby the aliphatic C−C links, on the left and on the right of the plot, corresponding to the green segments in Figure 2. The map at $z_2 \approx 0.94$ bohr shows a central

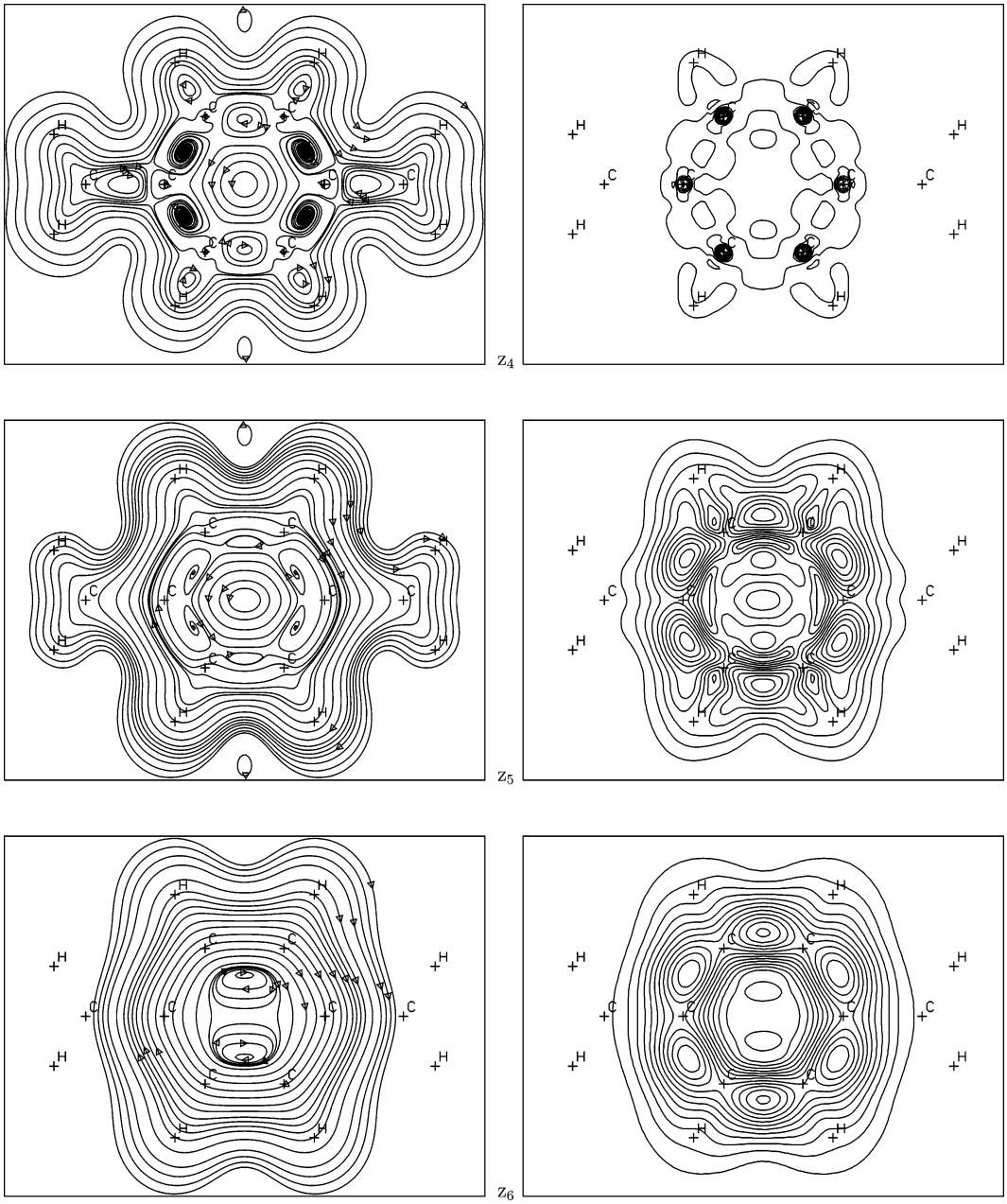

Figure 4. Plotting conventions are the same as in Figure 3. The contours are drawn from the initial value $|\mathbf{J^B}| = 0.0$ in steps of 1×10^{-2}, 8×10^{-2}, and 3×10^{-3} au to the maximum values 1.06×10^{-1}, 8.81×10^{-1}, and 3.67×10^{-2} au in the maps for z_4, z_5, and z_6, respectively.

paramagnetic vortex between two diamagnetic vortices. This pattern is contained in an extended domain of diatropic regime. Two small paramagnetic vortices can be observed on the left and on the right. They are separated from the central pattern by saddle points. This map nicely completes the information given by the SG of Figure 2.

Other plots of streamlines and moduli of $\mathbf{J^B}$ in planes at different heights $z_3 \approx 1.89$, $z_4 \approx 2.83$, $z_5 \approx 3.78$, and $z_6 \approx 4.72$ bohr along the central SL, is available in Figures 3 and 4. Interesting details can be found in these maps, illustrating different regimes along the vertical direction, e.g., the unfolding of the central paramagnetic vortex, of the diamagnetic vortices, and of spiral flow at opposite sides. They elucidate essential features of the ring current model for [2.2]paracyclophane and extend the concise information available from the SG of Figure 2. In particular, they show the persistence of the diatropic ring currents encompassing the whole molecule along the ϵ_3 direction. The portrait of a saddle is recognized in the central part of the last plot at z_6 (again, the aymptotes are not visible at the resolution adopted). Above and below the branching points at $z_6 \approx \pm 4.6$ bohr, the saddle regime takes place until the bifurcation points at $\pm Z$ are reached. Beyond them, the regime is vortical diamagnetic about the z axis.

4.2. Stagnation Graph for $\mathbf{B} \equiv B\epsilon_1$. The SG for a magnetic field parallel to the x axis through the midpoints of the aliphatic bridge bonds is shown in Figure 5. The primary SL coincides with the x direction. Paramagnetic vortical regime takes place in the proximity of the origin at CM. Branching of the (red) central SL occurs at two points on the x axis (at a distance $\approx \pm 0.35$ bohr from CM), where three stagnation lines originate: two (red) paramagnetic SLs forming a closed loop in the zx plane, and a (blue) segment of saddle SL, whose midpoint coincides with the origin. Above and below the central set of SLs, two undulating lines are observed. They have saddle character in the vicinity of the center of the phenylene units: vortical diamagnetic on crossing a C−C bridge, then saddle

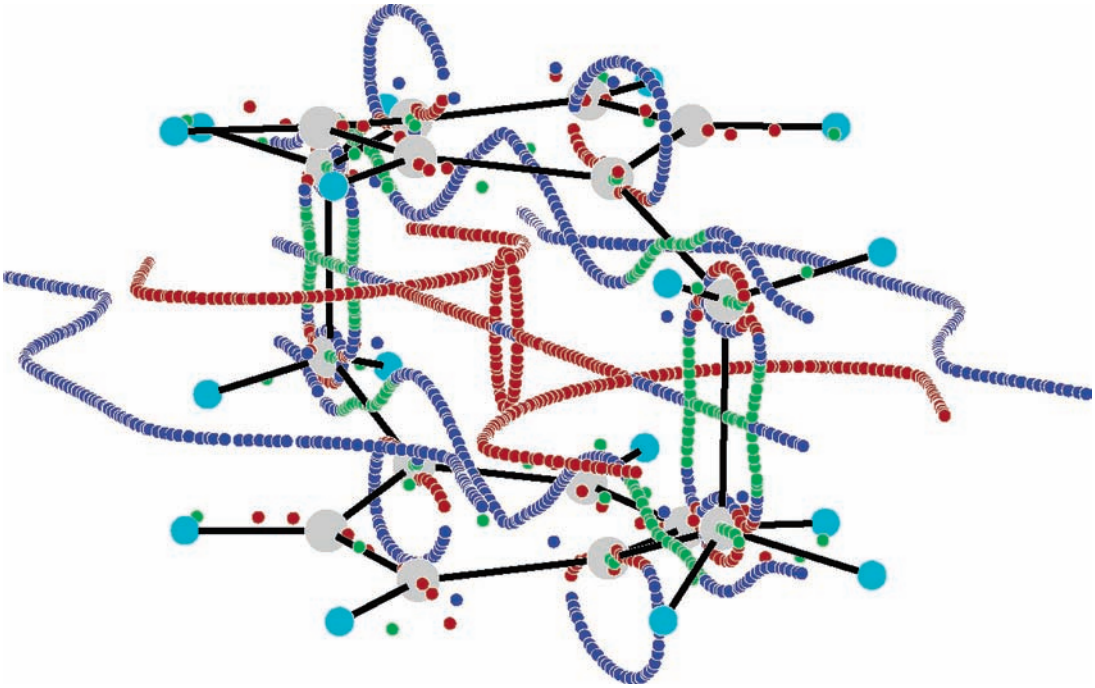

Figure 5. Perspective view of the stagnation graph of the current density vector field in [2.2]paracyclophane. The external magnetic field, $\mathbf{B} \equiv B\epsilon_1$, is parallel to the *x* axis passing through the midpoints of the central C−C bonds of the aliphatic bridges. Graphical conventions are the same as in Figure 2.

again up to the outer regions. This sequence of SLs is completely contained on the *zx* plane.

Two open red lines, also lying on the *zx* plane, indicate local vortical regime on opposite sides of the central paramagnetic loop. These SLs are truncated because the approximated wavefunction is insufficiently accurate in the external region. A larger basis set enriched by atomic functions on pseudocenters along the *z* direction would probably be necessary to improve the description, which is, however, beyond our present purposes.

Another couple of branching points is observed on the central SL at ≈±3.0 bohr from the origin, where the red line splits up into two red lines lying on the *xy* plane and a central saddle line connected to a closed loop on the *zx* plane in the basin of an aliphatic bridging bond. Each loop, on either side with respect to CM, contains a central green line bisecting an aliphatic C−C bond, which means that the local electron distribution sustains a diamagnetic vortex. This green line splits up into two green lines, belonging to the loop, and a central saddle line that extends to the tail regions. The loop contains also segments of saddle SL. The two branching points belonging to a given loop are found on the *x* axis, at ≈±4.5 and ≈±5.8 bohr from CM.

Four closed loops formed by saddle and paramagnetic vortical lines lie on the *zx* plane in the vicinity of carbons at the opposite ends of each aliphatic bridge. Two external continuous saddle SLs are observed on the *xy* plane, on either of CM. They go without interruption to the border of the map.

Plots of streamlines and moduli on *yz* planes normal to the B_x field, at distances $x_2 = 0.94$, $x_3 = 1.89$, $x_4 = 2.83$, $x_5 = 3.78$, $x_6 = 4.72$, $x_7 = 5.67$, and $x_8 = 6.61$ bohr from CM $\equiv x_1 = 0$, are given in Figures 6 and 7. The map through the origin of the coordinate system shows the central saddle, the two paramagnetic vortices above and below it along the *z* axis, then two external paramagnetic vortices corresponding to the truncated red lines in Figure 5. The two saddle points on the *z* axis, separating the central pattern from the external paramagnetic vortices on top and bottom of the map, belong to the blue SLs on the *zx* plane of the SG.

Four intense circulations are observed at the corners of the figure. They are not vortices (in fact no green SL is found in the SG of Figure 5). The flow spirals out in the electron-rich region around the C−C bonds of the phenylene units, and it is visible also in maps at a larger distance from CM. It is characterized by superimposed diamagnetic (clockwise) and paramagnetic (upward) components.

The map at x_2 describes the paramagnetic regime in a plane outside of the paramagnetic loop with center CM in the region between the branching points at ≈±0.35 and ≈±3.0 bohr. The spiralling flow at the corners is still very intense. The other plots give a clear visualization of the currents about the phenylene groups. Details are easily analyzed via the SG of Figure 5.

4.3. Stagnation Graph for $\mathbf{B} \equiv B\epsilon_2$. The SG for a magnetic field perpendicular to the *zx* plane of the aliphatic bridge bonds is shown in Figure 8. The regime is paratropic in the central part of the molecule up to the tail regions, as indicated by the central (red) vortical SL co-incident with the *y* axis, with the exclusion of a small domain containing the center of mass: saddlelike flow takes place about the blue segment, having the CM as midpoint. The opposite ends of this segment, at ≈±0.8 bohr from CM, are branching points where the central vortical SL splits up into two paramagnetic vortical lines, forming a closed loop that lies on the *yz* plane. This splitting of the central SL into two vortex and saddle SL fulfills the Gomes theorem.[24] Two open SLs, containing blue and green segments, lie on the *yz* plane, on either side of the central diamagnetic loop. The regime is saddlelike on crossing the C−C bonds of the phenylene rings and in the outer regions. On the *xy* plane, at opposite sides with respect to the CM, two closed loops, formed by saddle and paramagnetic vortical stagnation segments, are found. On the same plane, the SG shows that diamagnetic vortices flow nearby the midpoint of the central C−C bonds in each aliphatic bridge.

Maps of streamlines and moduli for selected planes perpendicular to the *y* axis, at distances $y_1 = 0$, $y_2 \approx 0.94$, $y_3 \approx 1.89$, $y_4 \approx 2.83 \approx$, and $y_5 \approx 4.05$ bohr, are shown in Figure 9. These

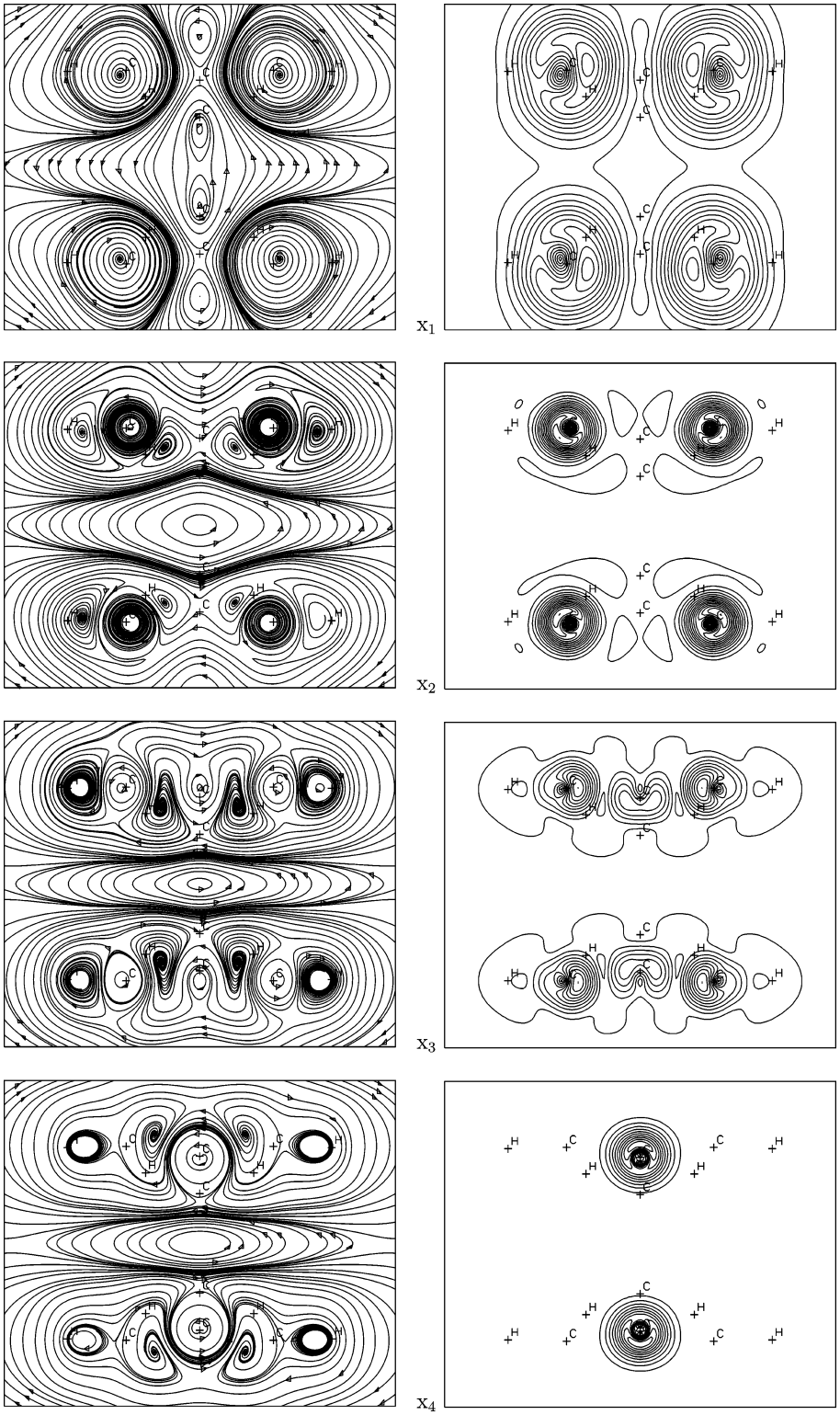

Figure 6. Streamlines (on the left) and contour levels for the modulus (on the right) of the current density $\mathbf{J^B}$ induced by a magnetic field $\mathbf{B} \equiv B\epsilon_1$ with intensity 1 au directed upward. On the *yz* plot planes, diamagnetic currents are clockwise. The distances x_i from the center of mass are specified in the Table. Atom positions are marked by crosses. The contours are associated with constant magnitude of $\mathbf{J^B}$, and are drawn from the initial value $|\mathbf{J^B}| = 0.0$ in steps of 4×10^{-3}, 2×10^{-2}, 3×10^{-2}, and 6×10^{-2} au to the maximum values 4.61×10^{-2}, 2.81×10^{-1}, 3.0×10^{-1}, and 6.39×10^{-1} au in the maps for $x_1 \ldots x_4$.

plots are easily analyzed with the help of the SG in Figure 8. The central region of paratropic regime is clearly visible through the whole series. In the map at $y_1 = 0$ bohr, the pattern illustrates the bifurcation of the central paramagnetic vortex line into two vortical lines and a saddle line in between, visible in Figure 8. The paramagnetic vortices next to the central pattern, left and right of it on the horizontal *x* axis, correspond to the red segments in the closed loops formed by red and blue SLs; see the analysis of the SG in Figure 8. The diamagnetic vortices on opposite sides of the *x* axis flow about the midpoints of the aliphatic C−C bridges; compare with the green SL in the same figure. Localized diamagnetic vortices are observed along the periphery of the system. Their spatial extension varies with the distance from the origin at CM.

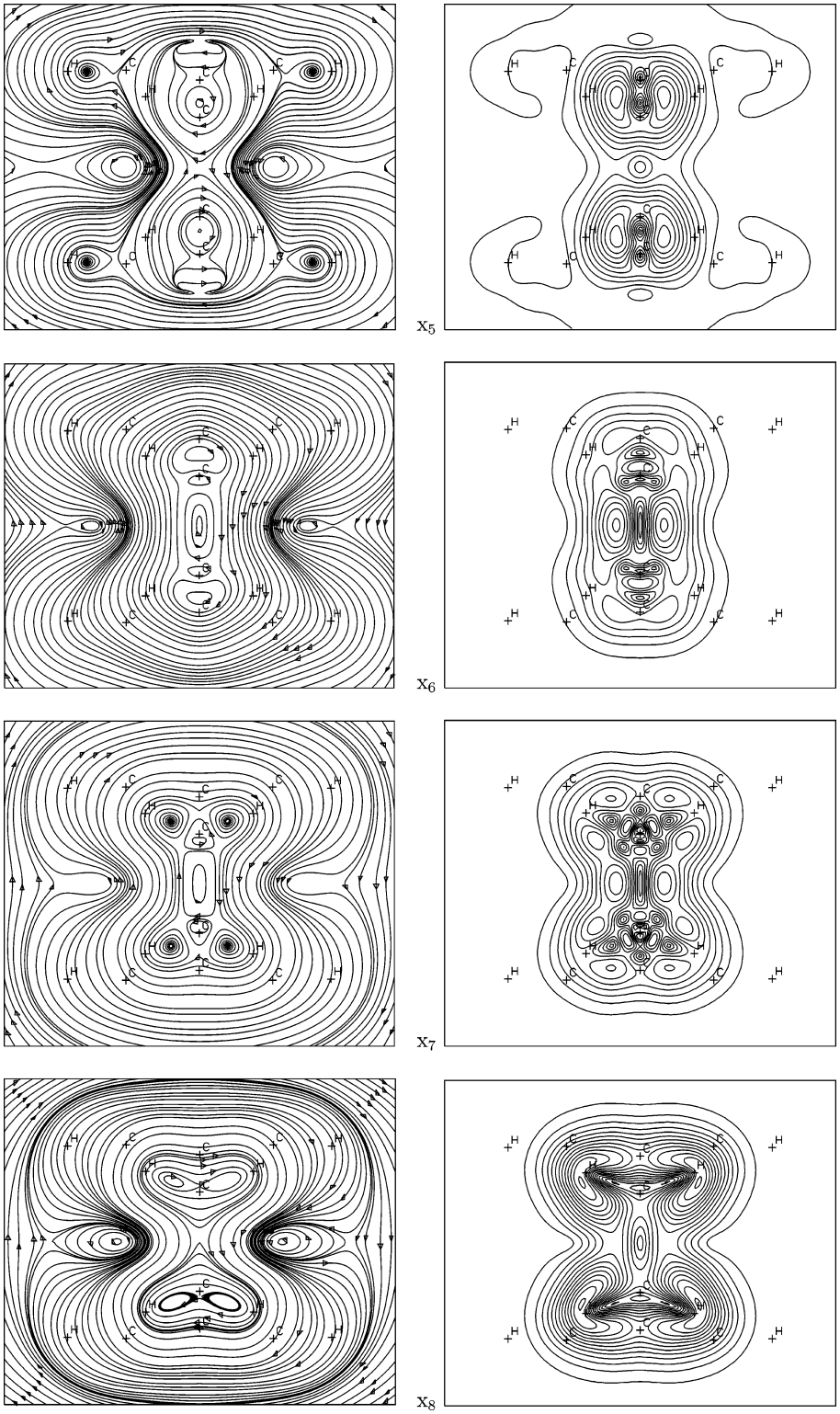

Figure 7. Plotting conventions are the same as in Figure 6. The contours are drawn from the initial value $|\mathbf{J^B}| = 0.0$ in steps of 4×10^{-3}, 7×10^{-3}, 1×10^{-2}, and 5×10^{-3} au to the maximum values 4.24×10^{-2}, 7.16×10^{-2}, 9.68×10^{-2}, and 6.58×10^{-2} au in the maps for x_5... x_8.

4.4. Rationalizing Magnetic Response via Stagnation Graphs. SGs and related current density maps are instrumental in understanding nuclear magnetic shielding. Let us consider the electronic current density $\mathbf{J^B}$, induced by an external magnetic field $\mathbf{B} \equiv B\epsilon_3$ in the electrons of a molecule, focusing on a closed circuit in the *xy* plane, which carries a diamagnetic (Larmor) current. The element of magnetic field induced at an observation point *P* on *xy*, at a distance **r** from d*V*, the volume which contains an element of electronic charge flowing in the circuit, is evaluated by the differential Biot−Savart law (DBSL)[17,20]

$$d\mathbf{B}_{ind}(r) = \frac{1}{c}\,\mathbf{J^B} \times \frac{\mathbf{r}}{|\mathbf{r}|^3}\,dV = -\,\mathbf{\Sigma}(r)\cdot\mathbf{B}\,dV \qquad (1)$$

denoting by $\mathbf{\Sigma}$ the magnetic shielding density[35,36] at the point *P*. The sign of the component $dB_{ind,z}$ depends on the sine of the angle between the vectors $\mathbf{J^B}$ and **r** (both lying on the *xy* plane),

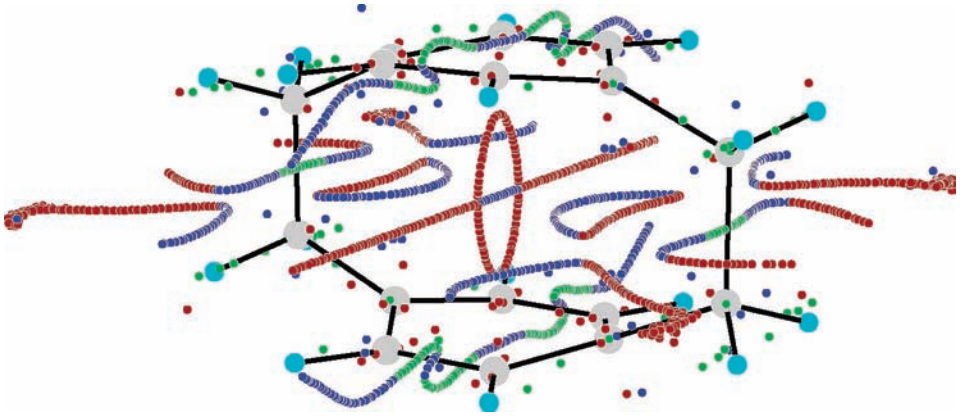

Figure 8. Perspective view of the stagnation graph of the current density vector field in [2.2]paracyclophane. The external magnetic field, $\mathbf{B} \equiv B\epsilon_2$, is parallel to the y axis perpendicular to the plane of the aliphatic bridges. Graphical conventions are the same as in Figure 2.

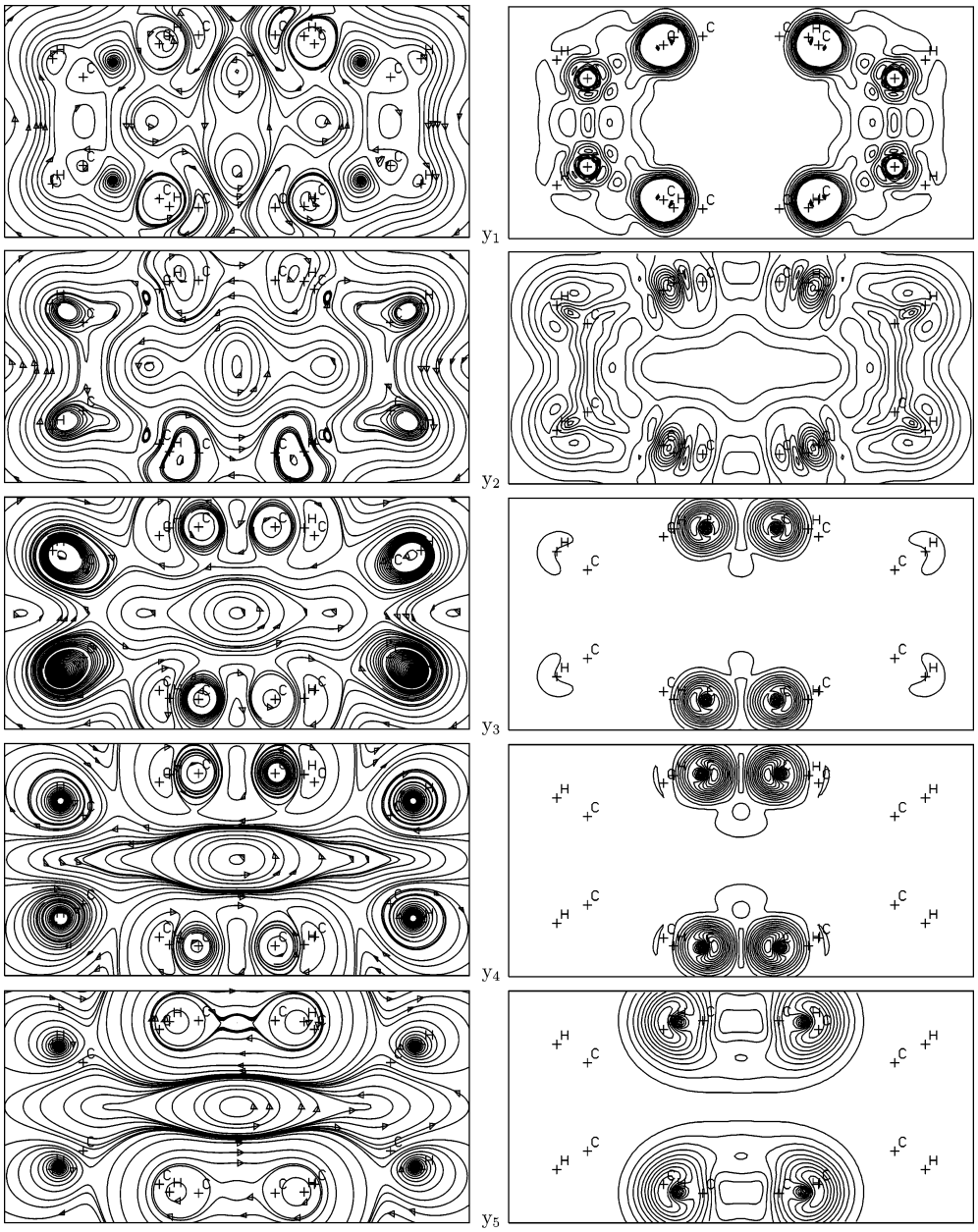

Figure 9. Streamlines (on the left) and contour levels for the modulus (on the right) of the current density $\mathbf{J^B}$ induced by a magnetic field $\mathbf{B} \equiv B\epsilon_2$ with intensity 1 au directed upward. On the xz plot planes, diamagnetic currents are clockwise. The distances y_i from the center of mass are specified in the Table. Atom positions are marked by crosses. The contours are associated with constant magnitude of $\mathbf{J^B}$, and are drawn from the initial value $|\mathbf{J^B}| = 0.0$ in steps of 2.5×10^{-2}, 1×10^{-2}, 4×10^{-2}, 2×10^{-2}, and 5×10^{-3} au to the maximum values 2.5×10^{-1}, 1.02×10^{-1}, 4.32×10^{-1}, 2.73×10^{-1}, and 5.37×10^{-2} au in the maps for $y_1 \ldots y_5$.

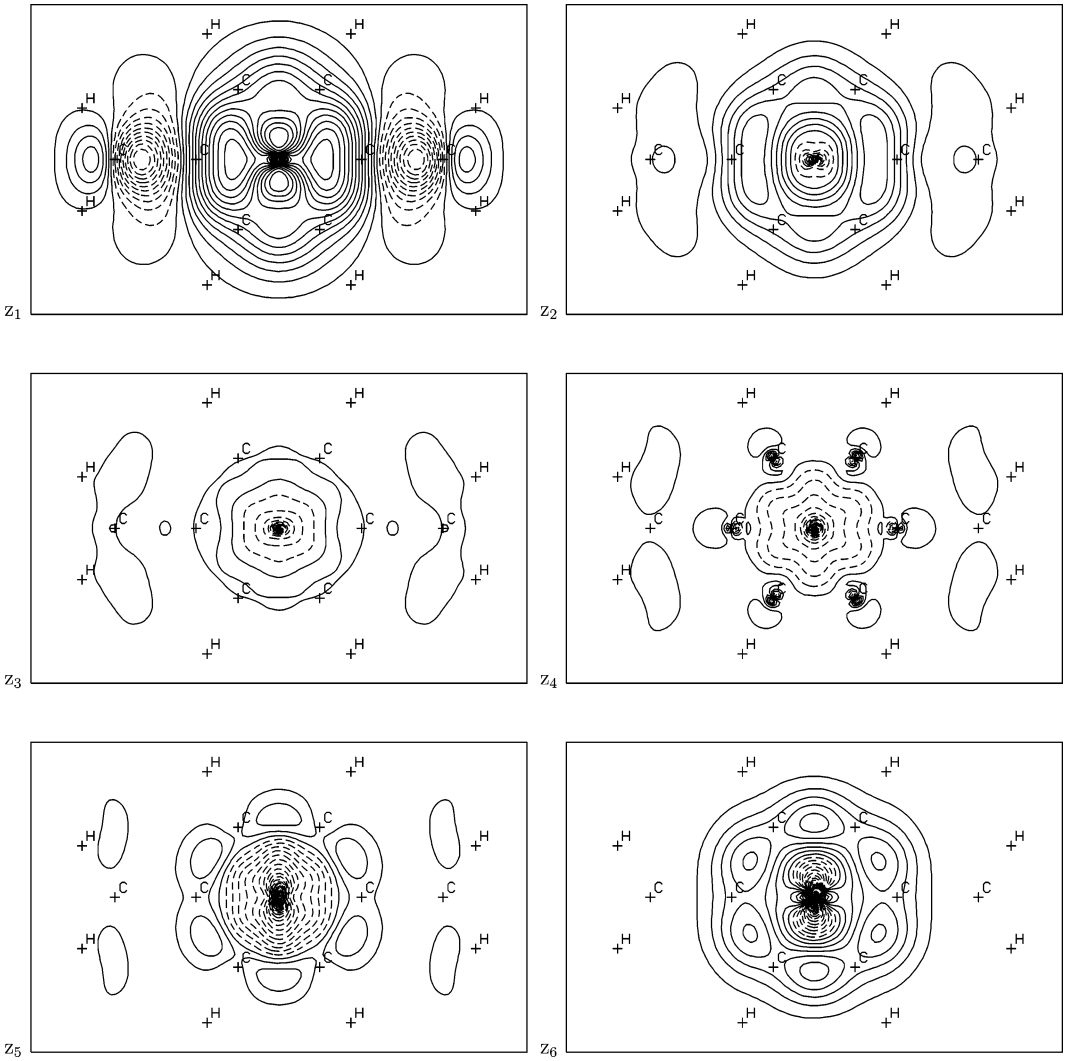

Figure 10. Shielding density obtained by the DBSL (eq 1) at points on the *z* axis, see the Table, induced by a magnetic field in the same direction. The contours are associated with constant magnitude of $\sum_{zz}$ and are drawn in steps of 2×10^{-4}, 1×10^{-3}, 1.5×10^{-2}, 2.0×10^{-2}, 5.0×10^{-3}, and 1×10^{-3} au in the maps for $z_1 ... z_6$.

thus the contribution from dV placed in a portion of the circuit closer to a probe, e.g., a proton H outside of it, with coordinates $\mathbf{R}_H$, reinforces the external field B_z by providing a positive $dB_{ind,z}(\mathbf{R}_H)$, so that the σ_{zz}^H component diminishes (paramagnetic shift). On the other hand, the distant portions of the circuit will induce negative contributions $dB_{ind,z}$ (R_H), enhancing σ_{zz}^H (diamagnetic shift).

As the contribution depends on the second inverse power of the distance of the probe from dV, according to eq 1, the total effect of a diamagnetic current loop L, with radius $\mathbf{r}_L$, on an external proton at distance $\mathbf{R}_H \gg \mathbf{r}_L$ is that of increasing the uniform magnetic field $\mathbf{B}$ by adding a local $\mathbf{B}(\mathbf{R}_H) \parallel \mathbf{B}$, thus decreasing the shielding σ_{zz}^H component.[17,20]

A diamagnetic current will induce a negative $dB_{ind,z}(\mathbf{r})$ at any point inside the circuit, causing a diamagnetic shift on a probe that would be placed at $\mathbf{r}$, i.e., providing a positive infinitesimal contribution to the local $\sigma_{zz}(\mathbf{r})$. At the center of a vortex, $\mathbf{J}^{\mathbf{B}}$ vanishes, e.g., a diamagnetic current proportional to $\mathbf{B} \times \mathbf{r}\, \rho(\mathbf{r})$, denoting by $\rho(\mathbf{r})$ the local electron charge density, goes to $\mathbf{0}$ as $\mathbf{r}$, whereas $\rho(\mathbf{r}) \neq 0$. If the origin of the coordinates coincides with the center of a diamagnetic loop, the DBSL magnetic shielding density $\sum$ defined by eq 1 diverges at the origin as $|\mathbf{r}|^{-1}$, and a positive spike is observed in the maps.

If the sign of the current $\mathbf{J}^{\mathbf{B}}$ flowing in the circuit is reversed, the sign of $dB_{ind,z}(\mathbf{R}_H)$ and $dB_{ind,z}(\mathbf{r})$ will also change. The sign of the shift of $\sigma_{zz}(\mathbf{R}_H)$ and $\sigma_{zz}(\mathbf{r})$ is also reversed.

4.4.1. Magnetic Shielding along the z Axis. Allowing for these simple rules, the SG can be used to analyze the trend of magnetic shieldings $\sigma_{zz}(\mathbf{r})$ along the z axis through the centers of the phenylene rings reported in the Table. The task is much facilitated by plotting the shielding density $\sum_{zz}$ defined in eq 1, see Figure 10.

These maps show the regions of molecular domain in which shielding/deshielding mechanisms are operating.[35,36] By superimposing the shielding density maps in Figures 10 to the corresponding streamline plots in Figures 3 and 4, the effect of the currents on magnetic shielding is easily understood via the DBSL (eq 1), according to the rules expounded above.

The shielding density on the xy plane at $z_1 = 0$ bohr provides a clear-cut explanation for the high value $\sigma_{zz} = 50.2$ ppm at CM. For any $\mathbf{r}$ within the central segment of saddle SL containing CM, the diatropic currents flowing all around enhance the out-of-plane component $\sigma_{zz}(\mathbf{r})$; compare with Figures 2 and 3. Weak deshielding arises only from the diamagnetic vortices in the region of the aliphatic carbon nuclei on the left and on the right of the map. It is caused by the portion of closed circuits closer to CM, whereas the more distant parts provide a small shielding contribution.

The variation of the $\sigma_{zz}(\mathbf{r})$ component of the central shielding at various distances $\pm z_i$ from the origin (see the Table) is interpreted analogously by the DBSL (eq 1). The values for $z_1...z_5$ decrease by increasing the distance from CM due to the downfield shift caused (i) by the portion of diamagnetic vortices closer to the *z* axis and (ii) by the central paramagnetic regime originating at the branching points $\approx\pm 0.4$ bohr, see the SG of Figure 2. Thus the σ_{zz} values at z_2 and z_3, 44.3 and 10.8 ppm, respectively, are smaller than that at z_1. The effect is documented by the sequence of shielding density maps at z_2-z_6. Stronger deshielding was found for z_5, where $\sigma_{zz}(\mathbf{r})$ is ≈ -3 ppm. Negative values, -2.5 and -2.1 ppm, were found also for z_4 and z_6, respectively.

Therefore, the variation along the *z* axis of $NICS_{zz}$, defined[4] as $-\sigma_{zz}(\mathbf{r})$, a problem unsolved so far,[8,9] is well understood via the spatial ring current model built via SG, streamlines, and shielding density maps.

4.4.2. Magnetic Shielding along the x and y Axes. Maps of shielding density $\sum_{xx}$, at various distances from the origin, along the *x* direction through the central aliphatic C−C bonds, are shown in Figure 11. The values of σ_{xx} on *yz* planes at $x_1,x_2,... x_8$ are reported in the Table. Allowing for the DBSL (eq 1), these estimates are easily interpreted by superimposing the shielding densities of Figure 11 to the corresponding plots of streamlines and moduli in Figures 6 and 7. The central part of the map at x_1 accounts for deshielding at CM caused by the (clockwise) diamagnetic component of strong currents spiralling about four C−C bonds of the phenylene moieties, and, to a lesser extent, by local paramagnetic flow of weak intensity. The map clearly evidences an abrupt change of sign of the $\sum_{xx}$ function. A closed continuous line through four C nuclei encompasses the deshielding domain. According to the rules quoted above, the element of field $dB_{ind,x}$, parallel (antiparallel) to the external B_x inside (outside) of this domain, is induced by the part of each spiralling circuit closer to (farther from) CM.

The map at $x_2 \approx 0.94$ bohr, Figure 6, shows four basins of strong spiral currents that flow anticlockwise along the direction of phenylene C−C bonds, i.e., in the opposite direction compared with the plane at $x_1 = 0$. Each anticlockwise spiral current lies between two weaker clockwise spirals; compare with the corresponding modulus map. The paramagnetic component of the intense anticlockwise currents gives a positive (negative) contribution to σ_{xx} at the origin arising from the portion closer to (farther from) it. The other shielding density maps of Figure 11 providing the information needed to interpret the change of the central shielding along the *x* direction, are similarly analyzed via the DBSL (eq 1).

The shielding density $\sum_{yy}$ on a few *zx* reference planes at distances $y_1,y_2,...y_5$ from CM (see the Table) are represented in Figure 12. They are analyzed by the same general rules for understanding the trend of σ_{yy}.

4.4.3. Magnetic Shielding of Phenylene Protons. Consider the phenylene proton H_1, with coordinates $\approx$(2.32, 4.05, 2.94). There is good agreement between theoretical predictions from CTOCD-PZ2 and GIAO methods, which indicates their accuracy. The calculated CTOCD-PZ2 components, $\sigma^H_{yy} \approx 23.9$ and $\sigma^H_{zz} \approx 23.4$ ppm, are very close to one another and smaller than $\sigma^H_{xx} \approx 27.2$ ppm. The average magnetic shielding σ^H_{Av} is as big as 24.8 ppm. A theoretical value $\delta^H \approx 6.3$ ppm for the chemical shift from tetramethylsilane (TMS) is obtained, allowing for the calculated value $\sigma^H_{Av} = 31.14$ ppm in TMS.[37] This is close to the experimental value 6.50 ppm quoted in the Supporting Information of the paper by Caramori et al.[8]

These results seem to imply that the downfield shift at phenylene protons attributable to π-ring currents is not significant. In fact, the estimate for σ^H_{zz} is bigger than that typical of aromatic systems by $\approx$ 3ppm (a near Hartree−Fock value for the deshielded out-of-plane component in benzene is 20.4 ppm[11]), and the average σ^H_{Av} is predicted 1.2 ppm bigger than that for benzene. Therefore, it can be safely concluded that the diatropism of [2.2]paracyclophane about the direction through the phenylene rings is smaller than that expected for a hypothetical model system containing two superimposed benzene molecules.

4.4.4. Magnetic Susceptibility. The SGs of [2.2]paracyclophane for different directions of the external magnetic field can be used to interpret also calculated values of the magnetic susceptibility tensor. The CTOCD-PZ2 predictions reported in the Table are $\chi_{xx} = -1017.6$, $\chi_{yy} = -998.0$, and $\chi_{zz} = -2708.6$ ppm cgs au per molecule (the conversion factor to ppm cgs emu per mole is $a_0^3/N = 8.9238878 \times 10^{-2}$, further conversion to SI units is obtained by 1 $JT^{-2} = 0.1$ cgs emu). These values are smaller than the corresponding GIAO by $\approx$ 2−5/% in absolute value.

The anisotropy $\Delta\chi = \chi_{zz} - (1/2)(\chi_{xx} + \chi_{yy}) = -1700.8$ ppm cgs au of the susceptibility tensor is quite big. The estimates are consistent with the spatial ring current model developed in this study. On the one hand, paramagnetic flow takes place in the central region and in the proximity of the C−C aliphatic bridges of [2.2]paracyclophane when the external magnetic field is directed as the *x* and *y* axes, as shown in Figures 5 and 8, reducing the magnitude of χ_{xx} and χ_{yy}. On the other hand, the diatropism of the molecule all along the *z* direction, documented by Figure 2 and by the maps in Figures 3 and 4, explains the enhanced value of χ_{zz}.

5. Concluding Remarks

Ring current models that represent the currents induced by an external magnetic field in the electrons of a big molecule on a few planes are in most cases insufficient to assess its magnetotropicity and to interpret its magnetic response. Planar models proposed so far become totally impractical in complex molecular systems such as [2.2]paracyclophane.

A powerful tool is available to build up *spatial* ring current models, i.e., a stagnation graph showing the set of points and lines at which the current density vanishes. Stagnation graphs yield a practical and abridged compendium of the essential information necessary to evaluate molecular magnetotropism all over the molecular domain by neatly showing the regions of diamagnetic and paramagnetic regime. They indicate the molecular basins in which maps of current density are needed to visualize the most representative phase portraits of the flow, i.e., vortices and saddles. Therefore stagnation graphs are valuable to assess local "magnetic" aromaticity and antiaromaticity.

The stagnation graphs obtained for the *x*, *y*, and *z* axes of a coordinate system visualize the currents induced by a uniform external magnetic field parallel to that direction. They help rationalize the components of tensor properties, e.g., magnetic susceptibility, magnetic shielding at the nuclei, and more generally, magnetic shielding at any point within the molecular dimensions.

Auxiliary tools are provided by maps of streamlines and moduli of the current density field. Plots of the shielding density defined via the differential Biot−Savart law can be combined with these maps to interpret magnetic shielding, by showing

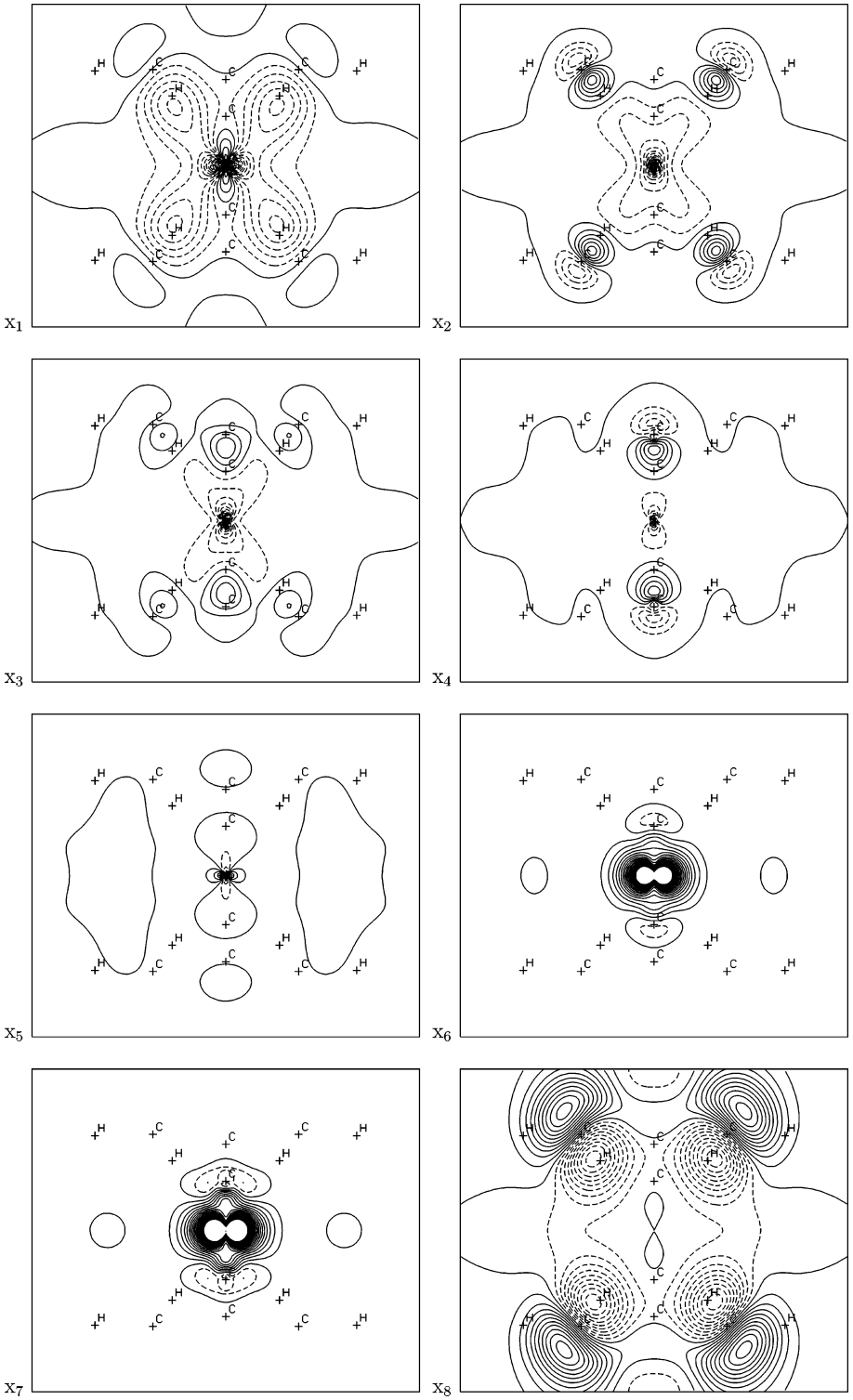

Figure 11. Shielding density obtained by the DBSL (eq 1) at points on the *x* axis, see the Table, induced by a magnetic field in the same direction. The contours are associated with constant magnitude of $\sum_{xx}$ and are drawn in steps of 1×10^{-3}, 4×10^{-3}, 1×10^{-2}, 2×10^{-2}, 3×10^{-2}, 2×10^{-1}, and 3×10^{-5} au in the maps for $x_1 ... x_8$.

the regions which provide contributions of different sign to this quantity at an arbitrary observation point.

The usefulness of stagnation graphs for practical purposes has been demonstrated in the present study of magnetic response of the [2.2]paracyclophane molecule, for which inconclusive results had been reported in the literature. Our investigation shows that a magnetic field directed as the axis through the phenylene rings (the "diatropism axis" of [2.2]paracyclophane) induces intense diamagnetic currents about it. However, this molecule is less diatropic than a hypothetical system formed by two superimposed benzene rings. Magnetic fields normal to the diatropism axis induce paratropic currents in some domain of the molecule, which substantially reduce its diamagnetism. Therefore, the absolute value of the corresponding components of magnetic tensors decreases.

The ring current model developed for [2.2]paracyclophane nicely accounts for the magnitude of measurable properties. The magnetic susceptibility is strongly anisotropic, the component

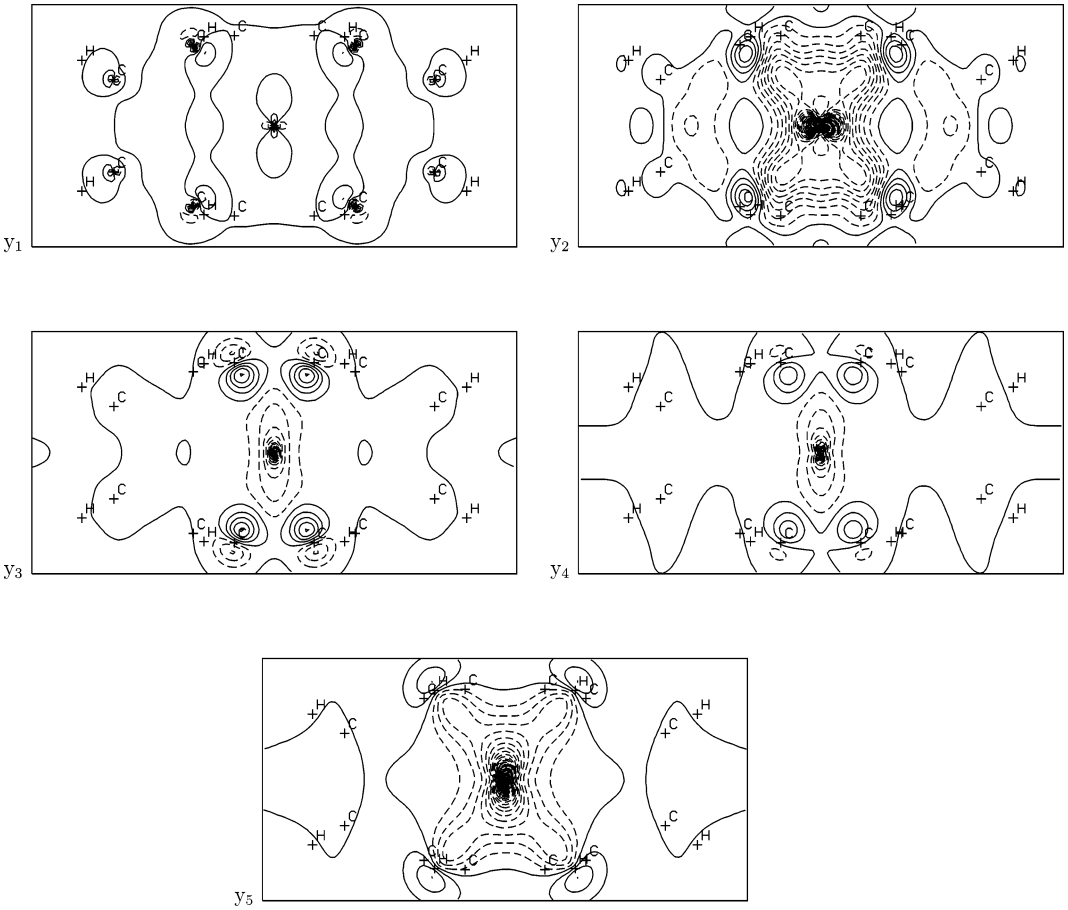

Figure 12. Shielding density obtained by the DBSL (eq 1) at points on the *y* axis, see the Table, induced by a magnetic field in the same direction. The contours are associated with constant magnitude of $\sum_{yy}$ and are drawn in steps of 2×10^{-2}, 1×10^{-3}, 1×10^{-2}, 1×10^{-2}, and 3×10^{-4} au in the maps for $y_1 ... y_5$.

corresponding to the diatropism axis being ≈2.7 times bigger (in absolute value) than the average component in orthogonal directions.

The average magnetic shielding at the phenylene protons is stronger than that of aromatics, the predicted upfield shift of [2.2]paracyclophane from benzene being as big as ≈1.2 ppm. This finding is in agreement with experimental data. It is consistent with the overall picture obtained via the stagnation graphs, but yields only a qualitative indication of decreased diatropicity with respect to the model of two superimposed benzene rings.

On the other hand, a reliable quantifier of reduced diatropicity is provided by the out-of-plane component of the phenylene proton shielding (i.e., corresponding to the direction normal to the plane of four equivalent ring carbon atoms). This is the unique quantity biased by π ring currents. It is approximately 3 ppm more shielded than the out-of-plane component of proton shielding in benzene, confirming that π ring currents are less intense in [2.2]paracyclophane.

Acknowledgment. Support from the European research and training network "Understanding Nanomaterials from a Quantum Perspective (NANOQUANT)'', contract no. MRTN-CT-2003-506842, and from the Italian MURST via PRIN funds, is gratefully acknowledged.

Supporting Information Available: LINUX and WINDOWS versions of the graphic code used to obtain three-dimensional representations of the stagnation graphs, the source for the stagnation graphs in Figures 2, 5, 8, and for the stagnation graph of the system of two superimposed benzene molecules. This material is available free of charge via the Internet at http://pubs.acs.org.

References and Notes

(1) Diederich, F. N. *Cyclophanes*; Stoddart, J. F., Ed.; Royal Society of Chemistry Monographs in Supramolecular Chemistry; Royal Society of Chemistry: Cambridge, U.K., 1991.

(2) Bickelhaupt, F. *Pure Appl. Chem.* **1990**, *62*, 373.

(3) Jones, C. J. *Chem. Soc. Rev.* **1998**, *27*, 289.

(4) von Ragué Schleyer, P.; Maerker, C.; Dransfeld, A.; Jiao, H.; van Eikema Hommes, N. J. R. *J. Am. Chem. Soc.* **1996**, *118*, 6317.

(5) Corminboeuf, C.; Heine, T.; Seifert, G.; von Ragué Schleyer, P.; Weber, J. *Phys. Chem. Chem. Phys.* **2004**, *6*, 273.

(6) Fallah-Bagher-Shaidaei, H.; Wannere, C. S.; Corminboeuf, C.; Puchta, R.; von Ragué Schleyer, P. *Org. Lett.* **2006**, *8*, 863.

(7) Chen, Z.; Wannere, C. S.; Corminboeuf, C.; Puchta, R.; von Ragué Schleyer, P. *Chem. Rev.* **2005**, *105*, 3842.

(8) Caramori, G. F.; Galembeck, S. E.; Lali, K. K. *J. Org. Chem.* **2005**, *70*, 3242.

(9) Poater, J.; Bofill, J. M.; Alemany, P.; Solà, M. *J. Org. Chem.* **2006**, *71*, 1700.

(10) Osuna, S.; Poater, J.; Bofill, J. M.; Alemany, P.; Solà, M. *Chem. Phys. Lett.* **2006**, *428*, 191.

(11) Lazzeretti, P. Ring Currents. In *Prog. Nucl. Magn. Reson. Spectrosc.*; Emsley, J. W., Feeney, J., Sutcliffe, L. H., Eds.; Elsevier: New York, 2000; Vol. 36, pp 1−88.

(12) Lazzeretti, P. *Phys. Chem. Chem. Phys.* **2004**, *6*, 217.

(13) Faglioni, F.; Ligabue, A.; Pelloni, S.; Soncini, A.; Viglione, R. G.; Ferraro, M. B.; Zanasi, R.; Lazzeretti, P. *Org. Lett.* **2005**, *7*, 3457.

(14) Lin, Y.-C.; Sundholm, D.; Jusélius, J. *J. Chem. Theory Comput.* **2006**, *2*, 761.

(15) Stanger, A. *J. Org. Chem.* **2006**, *71*, 883.

(16) Ferraro, M. B.; Lazzeretti, P.; Viglione, R. G.; Zanasi, R. *Chem. Phys. Lett.* **2004**, *390*, 268.
(17) Pelloni, S.; Ligabue, A.; Lazzeretti, P. *Org. Lett.* **2004**, *6*, 4451.
(18) Cuesta, I. G.; Ligabue, A.; de Merás, A. S.; Lazzeretti, P. *Chem. Phys. Lett.* **2005**, *401*, 282.
(19) Soncini, A.; Fowler, P. W.; Lazzeretti, P.; Zanasi, R. *Chem. Phys. Lett.* **2005**, *401*, 164.
(20) Ferraro, M. B.; Faglioni, F.; Ligabue, A.; Pelloni, S.; Lazzeretti, P. *Magn. Res. Chem.* **2005**, *43*, 316.
(21) Hirschfelder, J. O. *J. Chem. Phys.* **1978**, *68*, 5151.
(22) Fowler, P. W.; Steiner, E.; Havenith, R. W. A.; Jenneskens, L. W. *Magn. Res. Chem.* **2004**, *42*, S68.
(23) Gomes, J. A. N. F. *J. Chem. Phys.* **1983**, *78*, 4585.
(24) Gomes, J. A. N. F. *Phys. Rev. A* **1983**, *28*, 559.
(25) Gomes, J. A. N. F. *J. Mol. Struct. (THEOCHEM*) **1983**, *93*, 111.
(26) Pelloni, S.; Faglioni, F.; Zanasi, R.; Lazzeretti, P. *Phys. Rev. A* **2006**, *74*, 012506.
(27) Pelloni, S.; Lazzeretti, P. *Theor. Chem. Acc.* accepted for publication; DOI: 10.1007/s00214-006-0211-4.
(28) The LINUX and WINDOWS versions of the graphic code used to obtain three-dimensional representations of the stagnation graph and current density vector field of a series of molecules can be downloaded at https://theochem.chimfar.unimo.it/VEDO3/.
(29) Frisch, M. J.; Trucks, G. W.; Schlegel, H. B.; Scuseria, G. E.; Robb, M. A.; Cheeseman, J. R.; Zakrzewski, V. G.; Montgomery, J. A., Jr.; Stratmann, R. E.; Burant, J. C.; Dapprich, S.; Millam, J. M.; Daniels, A. D.; Kudin, K. N.; Strain, M. C.; Farkas, O.; Tomasi, J.; Barone, V.; Cossi, M.; Cammi, R.; Mennucci, B.; Pomelli, C.; Adamo, C.; Clifford, S.; Ochterski, J.; Petersson, G. A.; Ayala, P. Y.; Cui, Q.; Morokuma, K.; Malick, D. K.; Rabuck, A. D.; Raghavachari, K.; Foresman, J. B.; Cioslowski, J.; Ortiz, J. V.; Stefanov, B. B.; Liu, G.; Liashenko, A.; Piskorz, P.; Komaromi, I.; Gomperts, R.; Martin, R. L.; Fox, D. J.; Keith, T.; Al-Laham, M. A.; Peng, C. Y.; Nanayakkara, A.; Gonzalez, C.; Challacombe, M.; Gill, P. M. W.; Johnson, B. G.; Chen, W.; Wong, M. W.; Andres, J. L.; Head-Gordon, M.; Replogle, E. S.; Pople, J. A. *Gaussian 98*, revision A.7; Gaussian, Inc.: Pittsburgh, PA, 1998.
(30) Lazzeretti, P.; Malagoli, M.; Zanasi, R. Technical Report on Project "Sistemi informatici e calcolo parallelo'', Research Report 1/67; CNR: Rome, 1991.
(31) Zanasi, R. *J. Chem. Phys.* **1996**, *105*, 1460.
(32) van Duijneveldt, F. B. *Gaussian Basis Sets for the Atoms H-Ne for Use in Molecular Calculations*; Research Report RJ 945; IBM: San Jose, CA, 1971.
(33) Hansen, A. E.; Bouman, T. D. *J. Chem. Phys.* **1985**, *82*, 5035. This is the first reference in which the reinterpretation of the GIAO acronym for gauge-including atomic orbitals has been proposed, see footnote 6, p 5047.
(34) Angeli, C.; Bak, K. L.; Bakken, V.; Christiansen, O.; Cimiraglia, R.; Coriani, S.; Dahle, P.; Dalskov, E. K.; Enevoldsen, T.; Fernández, B.; Hättig, C.; Hald, K.; Halkier, A.; Heiberg, H.; Helgaker, T.; Hettema, H.; Jensen, H. J. A.; Jonsson, D.; Jørgensen, P.; Kirpekar, S.; Klopper, W.; Kobayashi, R.; Koch, H.; Ligabue, A.; Lutnaes, O. B.; Mikkelsen, K. V.; Norman, P.; Olsen, J.; Packer, M. J.; Pedersen, T. B.; Rinkevicius, Z.; Rudberg, E.; Ruden, T. A.; Ruud, K.; Salek, P.; Sánchez de Merás, A.; Saue, T.; Sauer, S. P. A.; Schimmelpfennig, B.; Sylvester-Hvid, K. O.; Taylor, P. R.; Vahtras, O.; Wilson, D. J.; Ågren, H. *Dalton, An Electronic Structure Program*, release 2.0; Dalton, 2005, (http://www.kjemi.uio.no/software/dalton/).
(35) Jameson, C. J.; Buckingham, A. D. *J. Phys. Chem.* **1979**, *83*, 3366.
(36) Jameson, C. J.; Buckingham,, A. D. *J. Chem. Phys.* **1980**, *73*, 5684.
(37) Cuesta, I. G.; de Merás, A. S.; Lazzeretti, P. *J. Comput. Chem.* **2006**, *27*, 1980.